Tạp chí Khoa học và Công nghệ, Số 74, 2025

HARMONIC REDUCTION FOR SINGLE-PHASE UNINTERRUPTIBLE POWER SUPPLY INVERTER

PHAM TRAN BICH THUAN[1], NGUYEN VINH QUAN*[2], TRAN THANH HAI[3]

[1] *Office of Science Management and International Affairs, Industrial University of Ho Chi Minh City, Ho Chi Minh City, Vietnam;*

[2] *Faculty of Electronics Technology, Industrial University of Ho Chi Minh City, Ho Chi Minh City, Vietnam;*

[3] *Office of Planning and Investment, Industrial University of Ho Chi Minh City, Ho Chi Minh City, Vietnam;*

**Corresponding author: quan_01037027@iuh.edu.vn*

DOIs: https://www.doi.org/10.46242/jstiuh.v74i2.5298

Abstract. Numerous control strategies for Uninterruptible Power Supply (UPS) inverters have been proposed, with the primary objectives of voltage tracking, stability, and maintaining a perfect sinusoidal waveform even under nonlinear loads, varying loads, and the presence of disturbances.
A proposed method is two Multiple Loop Control (MLC) with an outer voltage control loop tracking the reference voltage and an inner current control loop to reduce the steady-state error of the load voltage, reduce harmonics in the main circuit current, and improve system efficiency. The controller's robustness based on the Lyapunov function is proven by sudden load changes and variations in the reference voltage along with the presence of noise. The fundamental principles of Lyapunov's theorem are applied to the state equations to calculate the switching function for generating Pulse Width Modulation (PWM) to reduce harmonics in UPS.
Simulations and experiments were conducted using MATLAB-Simulink. Results demonstrated that the UPS output voltage and current can track the reference values from low to high, regardless of sudden load changes or reference voltage variations, and in the presence of noise. The total harmonic distortion (THD) of the current was significantly reduced to 0.04%, meeting the IEEE-519 standard.
Keywords. Uninterruptible Power Supply, Three-level inverter, Lyapunov.

1 INTRODUCTION

The primary objective of an uninterruptible power supply (UPS) system is to provide a sinusoidal voltage with constant amplitude and frequency to critical loads such as industrial controllers, computer systems, and communication systems without interruption, regardless of load conditions and supply variations [1, 2]. The main control in a UPS inverter is to track the output voltage to follow the desired sinusoidal waveform despite load changes or uncertainties inherent in the system [3, 4]. Achieving high performance, such as low total harmonic distortion (THD), good voltage regulation, and fast transient response to sudden load changes, is crucial in such applications [5-8].
Total harmonic distortion THD in voltage or current is determined by the following formula:

$$THD = \frac{\sqrt{\sum_{h>1}^{h_{max}} M_h^2}}{M_1} \times 100 \tag{1}$$

With h_{max} is the highest harmonic in the calculation, M_h is the rms value of the h^{th} harmonic and M_1 is the rms value of the fundamental component.
Harmonics can lead to various power quality problems:

a) High-frequency harmonics can cause voltage flicker, damaging equipment.
b) Generation of audible noise.
c) Increased core losses, leading to higher temperatures, reduced lifespan, and lower efficiency of electrical machines and transformers.
d) Resonance can occur, potentially shortening equipment life. The 5th and 7th harmonics create torque ripple in electric machines.

e) Magnetic and electric fields generated by harmonics can also interfere with telephone lines and other communication systems near the power system.

To address the aforementioned harmonics-related issues, various control techniques, including linear and nonlinear methods, have been implemented to achieve both good dynamic response and low THD at the UPS inverter output. However, they generally have the following advantages and disadvantages:

- Proportional-Integral (PI) and Proportional-Resonant (PR) controllers [9-11] are simple but lack robustness.
- Passive filters and power line conditioners [12-15] can reduce harmonics but have complex structures.
- Sliding Mode Control (SMC) provides a systematic approach to maintain stability, is insensitive to parameter variations and external disturbances, and does not require an accurate model. However, it has a high switching frequency, leading to chattering and potential damage to actuators [16-19].
- Fuzzy Logic Control (FLC) does not require accurate knowledge of load parameters [20-21], can handle nonlinearities without an accurate mathematical model, and has fast response and robustness to parameter variations and disturbances [22-23]. The algorithm is simple and can reduce both overshoot and settling time, but it has the disadvantage of fuzzy reasoning and requires powerful processing hardware.
- Neural Network Control (ANN) has the advantages of high adaptability and the ability to approximate nonlinear functions. A low-cost ANN control scheme for UPS inverters with a database containing all sampled data is proposed in [24]. In [25-26], an ANN application is presented for harmonics elimination, but the algorithm requires a large memory to generate PWM switching patterns for a given modulation index. ANNs are sensitive to load variations and uncertainties, requiring parameter estimation and have low stability.
- This paper proposes a Multiple Loop Control (MLC) algorithm to reduce harmonics in UPS applications. First, based on a mathematical model, the load voltage is controlled. Second, the system controls the current based on the Lyapunov function. This control method is one of the nonlinear control methods that provides excellent performance under large transients, not only with the fastest transient response to sudden changes but also ensuring system stability under all operating conditions [27-31].

This paper is structured as follows: Section 1 introduces the background and motivation of the research. Section 2 presents the mathematical model of the three-level cascade UPS inverter and formulates the control law design problem based on the Lyapunov function, proving the system stability. Section 3 presents simulation and experimental results, evaluating the normalized root mean square error (NRMSE) for measured quantities. Section 4 concludes the paper by highlighting the advantages of the proposed method and concludes with references.

2 THE PROPOSED CONTROLLER ALGORITHM

2.1 Mathematical model for UPS

Single-phase inverter with an LC filter is presented in Figure 1. On the left side of the single-phase H-bridge inverter is the DC voltage source, and on the right side is an unspecified load, connected through an LC filter. V_{dc} and S_1, S_2, S_3, S_4 represent the DC voltage source and four switches. The complementary states of the switches are:

$$S_1 + S_3 = 1, S_2 + S_4 = 1 \qquad (2)$$

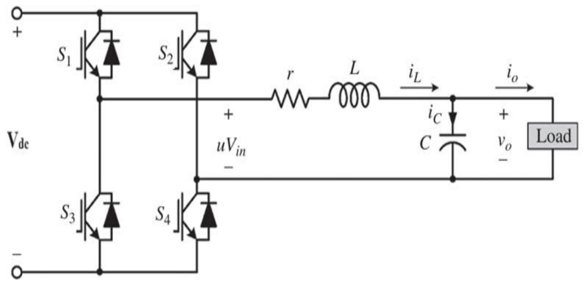

Figure 1: Single-phase inverter with output LC filter.

There are a total of four operating modes of the circuit, if n is the number of steps, the output voltage V_{in} of the H-bridge has three levels respectively $+V_{dc}$, $-V_{dc}$ and 0, which can be given as Table 1.

Table 1: Lock states

n	$[S_1, S_2]$	$V_{in} = (S_1 - S_2)V_{dc}$
0	[1, 0]	$+V_{dc}$
1	[1, 1], [0, 0]	0
2	[0,1]	$-V_{dc}$

Capacitor C and inductor L form a filter whose main function is to filter higher harmonics in the system current, the differential equation describing the inverter operation is given as follows:

$$L\frac{di_L}{dt} + ri_L = uV_{in} - v_0 \quad (3)$$

$$C\frac{di_0}{dt} + ri_L = i_L - i_0 \quad (4)$$

Where r is the resistance of the inductor L and u is a continuous signal in the closed range [-1, 1] that acts as the control input of the inverter system.
The control input is in the form of equation (5).

$$u = u_{sw} - u_{eq} \quad (5)$$

where u_{sw} and u_{eq} are the control inputs at equilibrium and the control near equilibrium, respectively. Assuming that the inductor current and capacitor voltage follow their set points well at steady state ($i_L = i_L^*$ and $v_0 = v_0^*$) and the control input is equal to the control input at steady state ($u = u_{sw}$), equations (3) and (4) can be rewritten as:

$$L\frac{di_L^*}{dt} + ri_L^* = u_{sw}V_{in} - v_0^* \quad (6)$$

$$C\frac{dv_0^*}{dt} + ri_L = i_L^* - i_0 \quad (7)$$

Let the state variables $x_2 = i_L^*$ and $x_1 = v_0^* - v_0$, then equations (6) and (7), (3) and (4) can be written:

$$L\frac{dx_2}{dt} = -u_{eq}V_{in} - rx_2 - x_1 \quad (8)$$

$$C\frac{dx_1}{dt} = x_2 \quad (9)$$

2.2 Lyapunov function based control design

The system stability is analyzed using Lyapunov stability theory, in the case of a single-phase inverter, the equilibrium point of interest is ($x_1 = 0, x_2 = 0$). The primary objective here is to achieve global asymptotic stability around this equilibrium point rather than local stability. This can be accomplished using the direct Lyapunov method, where the system states converge to the equilibrium point if the total energy is continuously dissipated. When the state trajectory reaches the equilibrium point, the energy dissipation converges to zero.

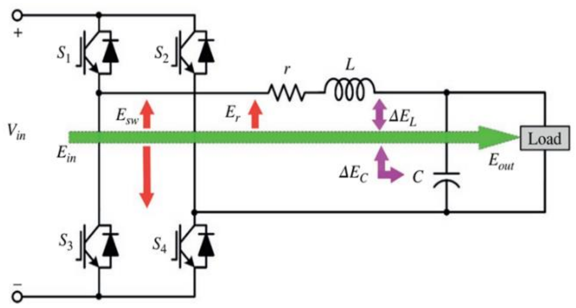

Figure 2: Power distribution in single phase inverter

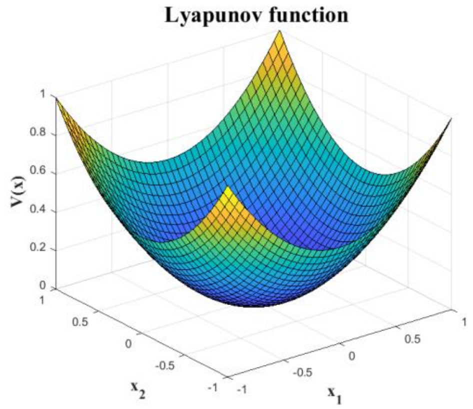

Figure 3: Lyapunov function in 3D surface

The typical power distribution of a single-phase inverter is depicted in Figure 2, where the input energy supplied by the DC source is denoted as E_{in}, and the energy dissipated by the inductor resistance and switching devices is denoted as E_r and E_{sw}, respectively. Therefore, while a portion of E_{in} is dissipated by the inductor resistance and switching devices, the remaining part of E_{in} is transferred to the load, denoted as E_{out}. Importantly, the energy stored in the inverter is distributed in the inductor and capacitor due to the fact that these passive components do not dissipate energy. Thus, a portion of Ein will be exchanged by the stored energy (ΔEL and ΔEC) in these components in both directions until the total dissipated energy stabilizes at the inverter's equilibrium point.

As known, the Lyapunov function must be an energy function as shown in Figure 3, implying that the Lyapunov function can be constructed by considering the stored energy in the inductor L and capacitor C in the inverter.

A typical Lyapunov function for different power inverters can be chosen as follows:

$$V(x) = \frac{1}{2}Cx_1^2 + \frac{1}{2}Lx_2^2 \tag{10}$$

Where x_1, x_2 are error variables.

It is clear from equation (10) that the Lyapunov function will include some terms in the form of stored energy in the inductor L and capacitor C respectively. The number of these terms depends on the mathematical model of the inverter under consideration.

The derivative of the Lyapunov function is given by:

$$\dot{V(x)} = x_1 C\dot{x}_1 + x_2 L\dot{x}_2 \tag{11}$$

Substitute equations (8) and (9) into (11) and we get:

$$\dot{V(x)} = -V_{in}x_2u_{eq} + rx_2^2 + d(t) \tag{12}$$

Where $d(t)$ is the random noise distribution function.

Obviously, if the u_{eq} control input is chosen to be:

$$u_{eq} = K_uV_{in}x_2,\ \ K_u > 0 \tag{13}$$

then the derivative of the Lyapunov function is always negative, that is,

$$\dot{V(x)} < 0 \tag{14}$$

Selected Lyapunov control law:

$$u = u_{sw} + u_{eq} = \frac{1}{V_{in}}\left(L\frac{di_L^*}{dt} + ri_L^* + v_0^*\right) + K_uV_{in}x_2 \tag{15}$$

Where the applied voltage and applied current v_0^* , i_L^* are given by equation (16, 17).

$$v_0^* = V_m\sin(2\pi ft) \tag{16}$$

$$i_0^* = C\frac{dv_0^*}{dt} + i_0 \tag{17}$$

When the inverter is controlled with law (15), the stability is guaranteed with the steady-state error of the output voltage, so the control law must add the feedback loop of the output voltage to the control loop. Therefore, the control law u_{eq} can be rewritten:

$$u_{eq} = K_u V_{in} x_2 - K_p x_1, \;\; K_p > 0 \tag{18}$$

Substitute equations (18) into (12):

$$V(\dot{x}) = -K_u V_{in}^2 x_2^2 - r x_2^2 + K_p V_{in} x_1 x_2 + d(t) \tag{19}$$

So $K_u > 0$ and $r > 0$, for equation (19) to be negative, K_p has its limit given by:

$$\frac{|D_{max}|}{V_{in} x_1 x_2} + K_p < \left(\frac{K_u V_{in}^2 + r}{V_{in}}\right)\frac{x_2}{x_1} \tag{20}$$

Where $|\, D_{max} \,|$ is the maximum amplitude of $d(t)$, which means that the closed-loop system is stable around $x = 0$.

The control law with output voltage feedback is as follows:

$$u = \frac{1}{V_{in}}\left(L\frac{di_L^*}{dt} + r i_L^* + v_0^*\right) + K_u V_{in} x_2 - K_p x_1 \tag{21}$$

The block diagram of the Lyapunov function is based control with output feedback voltage is depicted in Figure 4.

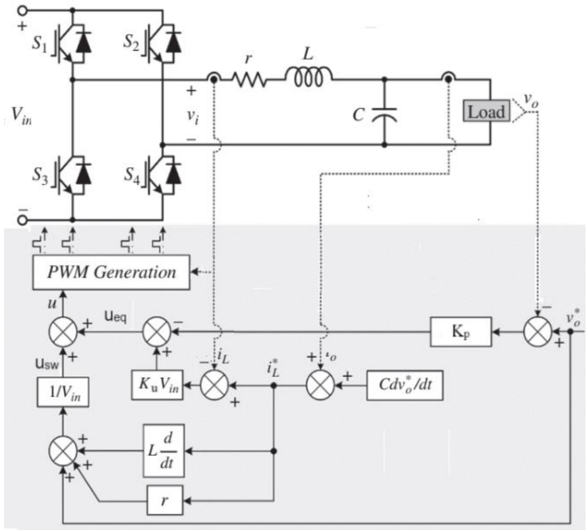

Figure 4: Generalized block diagram of the Lyapunov function based control of a UPS inverter.

2.3 Select control parameters

The performance of a control system is contingent upon the appropriate selection of its control parameters. Hence, a comprehensive study of the influence of control parameters on the closed-loop system is essential before implementation.

From equations (8), (9) and (18), we have the state matrix:

$$\frac{1}{V_{in}}\begin{bmatrix} x_1 \\ x_2 \end{bmatrix} = \begin{bmatrix} 0 & \frac{1}{C} \\ \frac{1}{L}\left(V_{in}K_p - 1\right) & -\frac{1}{L}\left(K_u V_{in}^2 + r\right) \end{bmatrix}\begin{bmatrix} x_1 \\ x_2 \end{bmatrix} \tag{22}$$

Characteristic equation of (22):

$$det(sI - A) = s^2 + \frac{1}{L}\left(K_u V_{in}^2 + r\right)s - \frac{1}{LC}\left(V_{in}K_p - 1\right) \tag{23}$$

With A is the 2×2 matrix in (22) and s denotes the Laplace operator. Applying the Routh-Hurwitz stability criterion, one can obtain the following condition:

$$\left(K_u V_{in}^2 + r\right) > 0, \; clearly\; K_u > 0 \tag{24}$$

$$\left(V_{in}K_p - 1\right) > 0 \; \rightarrow \; K_p > \frac{1}{V_{in}} \tag{25}$$

2.4 Pulse width modulation (PWM)

PWM pulse width modulation is generated from the comparison between the control law u and the hysteresis threshold h. Equations (26) and (27) use the dual-band hysteresis modulation scheme to have three levels of the inverter output voltage:

$$S_1 = \begin{cases} 1 & if\ x = u < +h \\ 0 & Otherwise \end{cases} \tag{26}$$

$$S_2 = \begin{cases} 1 & if\ x = u > -h \\ 0 & Otherwise \end{cases} \tag{27}$$

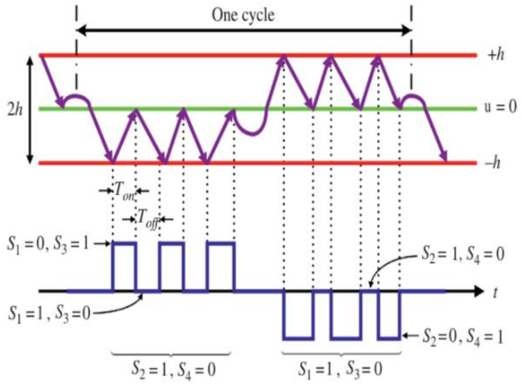

Figure 5: Dual-band delay switching in one cycle.

HW - Hysteresis Switching is illustrated in Figure 5. It is clear that the control law u changes between the upper and lower boundaries of the hysteresis threshold h.

Table 2: Switching Logic.

	Condition	$[S_1, S_2, S_3, S_4]$
Positive half-cycle of u	u < +h	[1,0,0,1], $+V_{dc}$
Negative half-cycle of u	u > -h	[0,1,1,0], $-V_{dc}$
	u > 0, u < 0	[1,1,0,0], 0V

Table 2 details the switching logic where h represents the dead time. During a positive half-cycle, S_1 and S_3 switch, while S_2 and S_4 switch during the negative half-cycle. This dual-band dead-time scheme results in equal switching losses for all devices per cycle. Additionally, while S_3 and S_4 have continuous conduction losses, S_1 and S_2 only incur conduction losses during their switching transitions.

3 SIMULATION AND EXPERIMENTATION

Simulation and experimental results were conducted on MATLAB/Simulink with a sampling time of $T_s = 10\mu s$ and the parameters are given in Table 3. The results will evaluate the compatibility between the reference signal y^* and the measured signal y, given by equation (28), where $mean(y)$ is the mean value of y.

$$NRMSE = 100\left(1 - \frac{\|y^* - y\|}{\|y^* - mean(y^*)\|}\right) \tag{28}$$

The goal is to develop a robust controller that ensures stability around the operating point and achieves high dynamic performance, characterized by limited overshoot, settling time, and output harmonics, under varying input voltage and load conditions.

System performance is assessed under three scenarios: changes in reference voltage v_0^*, variations in load resistance R, and the presence of unmodeled disturbances, including random noise d(t). The results demonstrate the tracking performance of the output voltage and inductor current for varying v_0^* and R, and the THD and NRMSE values for voltage and current are analyzed. The solid red line in the plots represents the reference values v_0^*, i_L^*, and the dashed blue line represents the measured values v_0, i_L.

Table 3: Simulation and experimental parameters.

Symbol	Value
DC link voltage, V_{in}	400 V
Set value, v^*_o	$220\sqrt{2}$ V
Inductance, L	5 mH
Filter capacitance, C	50 µF

Load resistance, R	100 Ω
Inductor resistance, r	0.067 Ω
Current gain, K_u	0.1
Voltage gain, K_p	100
Band hysteresis, h	30
Time sampling, T_s	10μs

3.1 Simulation results

The simulation and experimental results in Figure 6 validate the effectiveness of the proposed control algorithm. The control system comprises two loops: an outer voltage loop with a proportional gain $K_p x_1$ to ensure that the load voltage v_0 tracks the reference voltage v_0^*, and an inner current loop to regulate the input current i_L to track the reference current i_L^*, thereby minimizing inverter losses.

The results show that the controller achieves the desired performance objectives, including excellent tracking of the reference signals v_0^* and i_L^*, and low output harmonics. The NRMSE values for both voltage and current further confirm the high accuracy of the control system. The Lyapunov-based inner control loop generates the PWM signals, ensuring system stability and maintaining the system at the equilibrium point.

Figure 7 shows the output voltage of the inverter when using the dual-band delay modulation scheme, with three voltage levels -400 V, 0 V and +400 V.

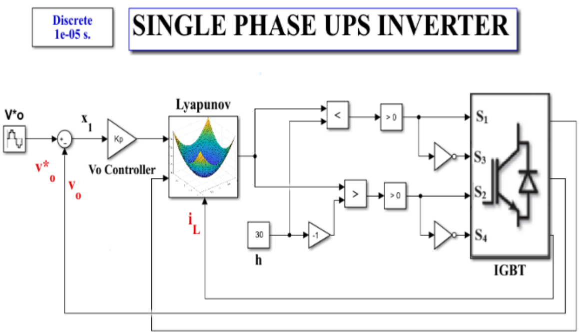

Figure 6: Simulink diagram for ups inverter.

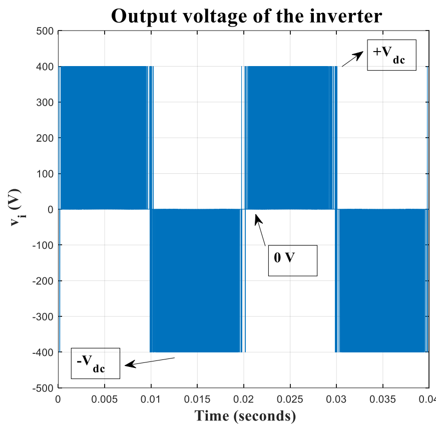

Figure 7: Output voltage of third-order inverter

Figure 8 shows that when $v_0^* = 220\sqrt{2}\,V$, the measured voltage v_0 tracks the reference value accurately, and the inductor current i_L also follows its reference value closely, reaching approximately 6A for a load resistance R = 100Ω. Notably, both voltage and current exhibit a sinusoidal waveform with very low THD, indicating high tracking accuracy and the effectiveness of the proposed algorithm. The corresponding NRMSE and THD values for voltage and current are [98.43%, 93.18%] and [0.04%, 06.24%], respectively.

Figure 9 shows that when $v_0^* = 110\sqrt{2}\,V$, the measured output voltage v_0 tracks the reference value accurately, and the inductor current i_L reaches a steady-state value of approximately 3A. The corresponding NRMSE and THD values for voltage and current are [98.42%, 87.23%] and [0.086%, 12.33%], respectively, indicating high tracking accuracy and low harmonic distortion.

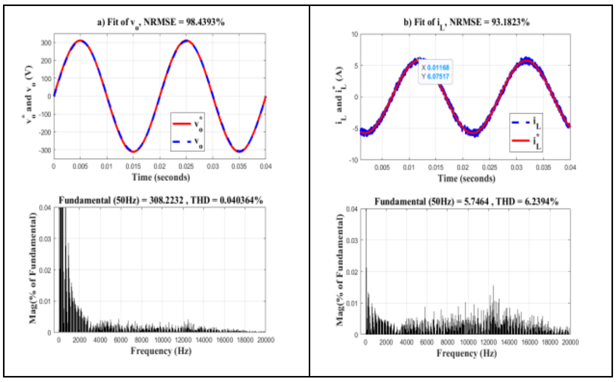

Figure 8: The corresponding v_0 and i_L when $v_0^* = 220\sqrt{2}\,V$

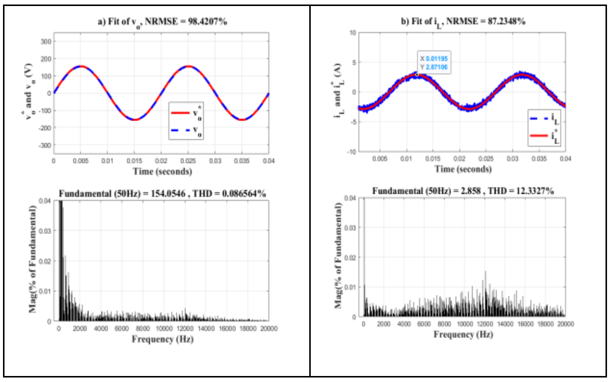

Figure 9: The corresponding v_0 and i_L when $v_0^* = 110\sqrt{2}\,V$

Figure 10 illustrates that when $v_0^* = 50\sqrt{2}\,V$, the measured output voltage v_0 accurately tracks the reference value, and the inductor current i_L reaches a steady-state value of approximately 1.5A. The voltage and current waveforms exhibit low THD values of 0.21% and 24.20%, respectively, indicating good tracking performance and the compatibility always reaches NRMSE value > 98%. Figure 11 demonstrates the robustness of the proposed control algorithm under disturbances. When ±8V disturbance is introduced into the DC voltage V_{dc}, the load current io remains sinusoidal with a low THD of 0.039%, indicating excellent disturbance rejection capabilities.

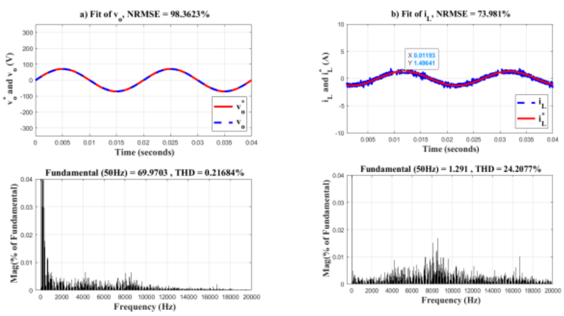

Figure 10: The corresponding v_0 and i_L when $v_0^* = 50\sqrt{2}\,V$

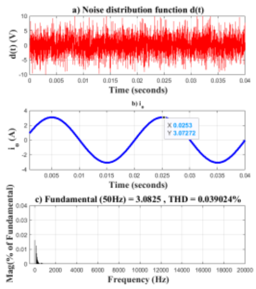

Figure 11: Noise distribution $d(t)$, i_0 and THD of i_0

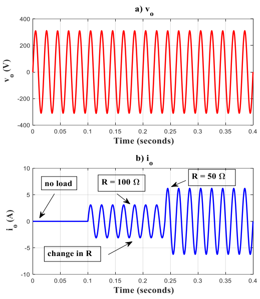

Figure 12: The corresponding v_0 and i_L with step change of load $R = \infty, 100\Omega, 50\Omega$

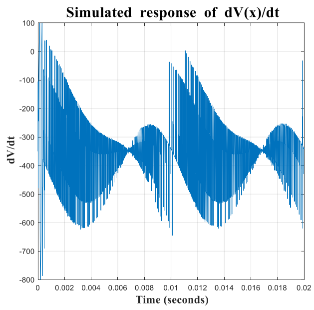

Figure 13: *Simulated response of dV(x)/dt*

Figure 12 shows the system response to a step change in load resistance from an open circuit (0.1 s) to 100 Ω (0.15 s) and then to 50 Ω (0.15 s). The output voltage v_0 accurately tracks the reference value, while the load current i_0 adapts to the changing load resistance. The results demonstrate the system's robustness and ability to maintain stability under varying load conditions. Figure 13 shows the simulation result of $dV(x)/dt$ within one cycle (0.02s) corresponding to the step change in load resistance presented in Figure 12. The negative value of $dV(x)/dt$ for all load conditions confirms the global asymptotic stability of the closed-loop system.

3.2 Experimental results

Figure 14 shows the real-time experimental setup for the UPS inverter. The control algorithm is implemented on MATLAB/Simulink, and the converter's response is acquired on a PC through a DSP 320F28379 card. The reference voltage v_0^* is adjusted using a 1KΩ potentiometer.

Figure 15 presents the experimental output voltage waveform of the inverter using the dual-band dead-time scheme with three voltage levels: -400 V, 0 V, and +400 V. The observed voltage level overlap is attributed to the dead-time mismatch in the practical implementation.

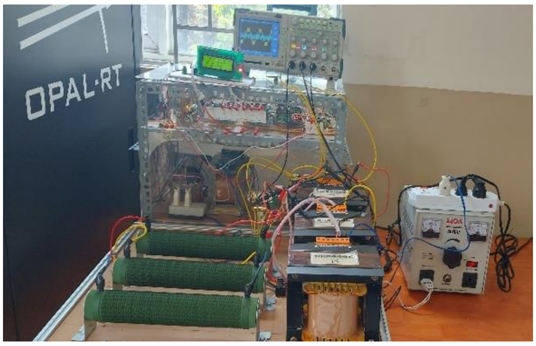

Figure 14: Experimental setup.

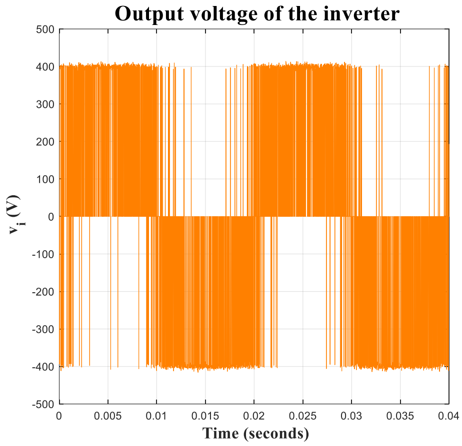

Figure 15: The experimental output voltage waveform of the inverter

Figure 16 presents the experimental results for $v_0^* = 220\sqrt{2}\,V$ and $R = 100\Omega$. The measured output voltage v_0 and inductor current i_L closely follow their respective reference values, with i_L reaching approximately 6A. Both voltage and current exhibit sinusoidal waveforms with high tracking accuracy, as indicated by the NRMSE values of 98.42% and 88.89% for voltage and current, respectively. The low THD values of 0.10% and 10.56% further confirm the excellent performance of the proposed control algorithm. Figure 17 presents the experimental results for $v_0^* = 110\sqrt{2}\,V$. The measured output voltage v_0 accurately tracks the reference value, and the inductor current i_L reaches a steady-state value of approximately 3A. The voltage and current waveforms exhibit sinusoidal characteristics with high tracking accuracy, as indicated by the NRMSE values of 98.42% and 78.02% for voltage and current, respectively. The low THD values of 0.2% and 21.68% .

Figure 18 presents the experimental results for $v_0^* = 110\sqrt{2}\,V$. The measured output voltage v_0 accurately tracks the reference value, and the inductor current i_L reaches a steady-state value of approximately 1.5A. The voltage and current waveforms exhibit sinusoidal characteristics with high tracking accuracy, as indicated by the NRMSE values of 98.37% and 53.05% for voltage and current, respectively. The low THD values of 0.42% and 45.25% further confirm the excellent performance of the proposed control algorithm.

Figure 19 presents the experimental load current io under ±8V disturbance in the DC voltage V_{dc}. The load current exhibits a sinusoidal waveform with a very low THD of 0.09%, demonstrating the high quality of the output signal and the effectiveness of the control algorithm in rejecting disturbances.

The experimental results in Figure 20 verify the global asymptotic stability of the closed-loop system. The plot shows the time derivative of the state variable x, $dV(x)/dt$, for a step change in load resistance. The consistently negative values of $dV(x)/dt$, regardless of the load resistance, confirm the theoretical analysis and demonstrate the system's robustness.

Figure 21 compares the simulated and experimental results, highlighting the differences in NRMSE and THD. The discrepancies can be attributed to the non-ideal characteristics of real-world components and the presence of external disturbances. While the output voltage v_0 shows good agreement between simulation and experiment, the inductor current i_L exhibits some differences, particularly in terms of THD. These discrepancies can be attributed to factors such as parameter variations and unmodeled dynamics.

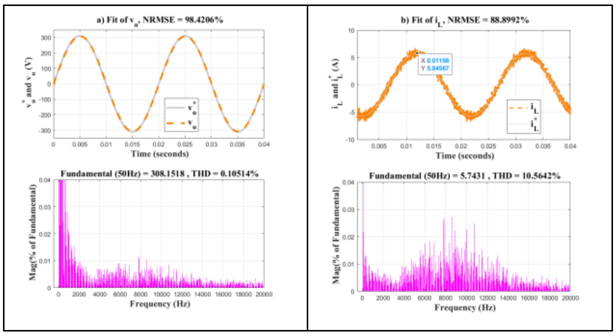

Figure 16: The corresponding v_0 and i_L when $v_0^* = 220\sqrt{2}\,V$

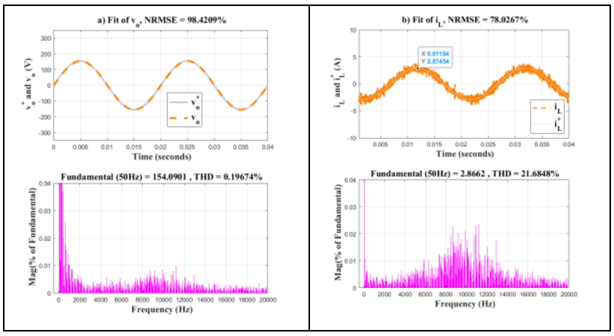

Figure 17: The corresponding v_0 and i_L when $v_0^* = 110\sqrt{2}\,V$

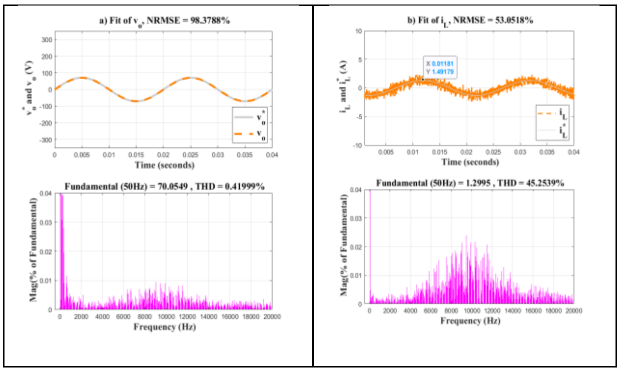

Figure 18: The corresponding v_0 and i_L when $v_0^* = 50\sqrt{2}\,V$

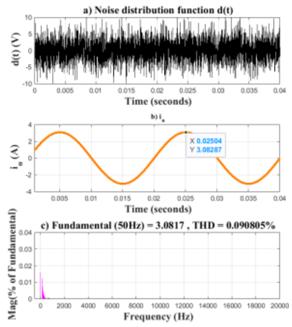

Figure 19: Noise distribution $d(t)$, i_0 and THD of i_0

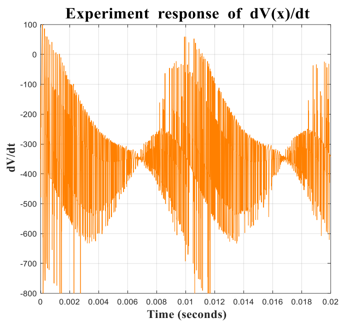

Figure 20: Experiment response of $dV(x)/dt$.

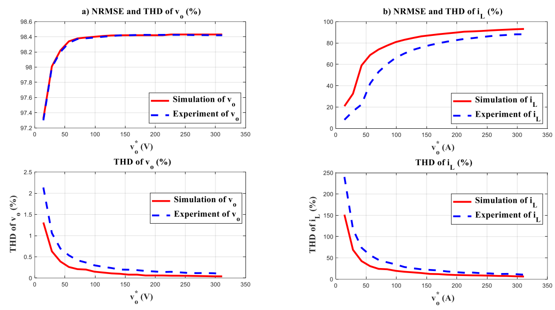

Figure 21: Comparison between simulation and experiment of v_0 and i_L when v_0^* changes

4 CONCLUSIONS

Simulation and experimental results have clearly demonstrated the effectiveness of the proposed dual-loop Lyapunov-based control strategy for single-phase inverters. The controller exhibits exceptional performance in tracking the reference values of both voltage and current, even under varying load conditions and in the presence of disturbances. The Lyapunov-based approach ensures the global asymptotic stability of the system, guaranteeing that the system converges to the equilibrium point regardless of initial conditions.

The results also show that the proposed controller is suitable for nonlinear systems, the most outstanding feature of the method is that it is completely insensitive to the uncertainties and external noises entering the system during the control process, the method makes the system asymptotically stable around the equilibrium point $V(x) = 0$ when $x = 0$, and away from its equilibrium point $V(x) > 0$ when $x \neq 0$, the system will be stable and maintain it in a stable state.

ACKNOWLEDGMENT

This work was supported by Industrial University of Ho Chi Minh City, Vietnam (IUH). The authors would like to thank IUH, the editor, the associate editors and the reviewers for their valuable comments.

REFERENCES

[1]. F.S. Pai, S.J. Huang, A novel design of line interactive unint- erruptible power supplies without load current sensors, *IEEE Trans. On Pow. Elec.*, Vol.21, No.1, pp.202-210, Jan. 2006.

[2]. J. Faiz, G. Shahgholian, "Uninterruptible power supply", *A review ELECTOMOTION*, Vol.13, No.4, pp. 276-289, Nov./Dec. 2006.

[3]. G. Escobar, A.A. Valdez, J.L. Ramos, P. Mattavelli, Repetitive based controller for a UPS inverter to compensate unbalance and harmonic distortion, *IEEE Trans. On Indu. Elec.*, Vol.54, No.1, pp.504-510, Feb. 2007.

[4]. M. Niroomand, H.R. Karshenas, Performances specifications of series-parallel UPS' s with different control strategies, *International Review of Electrical Engineering (IREE)*, Vol. 4, No. 1, pp. 14-21, Feb. 2009.

[5]. Y. H. Chen, P.T. Cheng, Flux estimation techniques for inrush current mitigation of line-interactive UPS systems, *IEEE Trans. on Ind. Appl*., Vol.47, No.2, pp.901-911, March-April 2011.

[6]. L. Bouslimi, A. Chammam, M. Ben Mustapha, M. Stambouli, J.P. Cambronne, Simulation and experimental study of an electronic pulsed power supply for HID lamps Intended for photochemical applications, *International Review of Electrical Engineering*, Vol. 4, No. 5 (Part A), pp. 799-808, Oct. 2009.

[7]. Y.H. Chen, P.T. Cheng, An inrush current mitigation technique for the line-interactive uninterruptible power supply systems, *IEEE Trans. on Ind. Appl*., Vol.46, No.4, pp.1498-1508, July- Aug. 2010.

[8]. R. Senthil Kumar, J. Jerome, P. Prem, T. Alex Stanley Raja, Soft switched four wire inverter for UPS applications, *International Review of Electrical Engineering*, Vol. 5, No. 4 (Part A), pp.1405-1412, Aug. 2010.

[9]. Castilla, M.; Miret, J.; Matas, J.; Vicuna, L.G.D.; Guerrero, J.M. Control Design Guidelines for Single-Phase Grid-Connected Photovoltaic Inverters With Damped Resonant Harmonic Compensators. *IEEE Trans. Ind. Electron*. 2009, 56, 4492–4501.

[10]. Chen, D.; Zhang, J.M.; Qian, Z.M. An Improved Repetitive Control Scheme for Grid-Connected Inverter With Frequency-Adaptive Capability. *IEEE Trans. Ind. Electron*. 2012, 60, 814–823.

[11]. Trinh, Q.N.; Lee, H.H. An Enhanced Grid Current Compensator for Grid-Connected Distributed Generation Under Nonlinear Loads and Grid Voltage Distortions. *IEEE Trans. Ind. Electron*. 2014, 61, 6528–6537.

[12]. D. Buła, D. Grabowski, and M. Maciazek, "A review on ˙ optimization of active power filter placement and sizing methods," *Energies*, vol. 15, no. 3, p. 1175, 2022.

[13]. A. A. Sallam and O. P. Malik, "Harmonics effect mitigation," *in Electric Distribution Systems*, pp. 403–428, IEEE, Man- hattan, NY, U. S. A, 2019.

[14]. K. S. Alam, D. Xiao, D. Zhang, and M. F. Rahman, "Single- phase multicell AC-DC converter with optimized controller and passive filter parameters," *IEEE Transactions on Industrial Electronics*, vol. 66, no. 1, pp. 297–306, 2019.

[15]. Y. Yang, L. Wang, and H. Sun, "A design of PWM inverter passive filter based on CM transformer," CPSS *Transactions on Power Electronics and Applications*, vol. 5, no. 2, pp. 180–190, 2020.

[16]. N.Vazquen, J.Alvarez, C.Aguilar, J.Arau, "Some critical aspects in sliding mode control design for the boost inverter", *IEEE/CIEP*, pp.76-81, 1998.

[17]. J.F.Silva, S.S.Paulo, "Fixed frequency sliding modulator for current mode PWM inverters", *IEEE/PESC*, pp.623-629, June 1993.

[18]. Zheng, L.J.; Jiang, F.Y.; Song, J.C.; Gao, Y.G.; Tian, M.Q. A Discrete -Time Repetitive Sliding Mode Control for Voltage Source Inverters. *IEEE J. Emerg*. Sel. Top. Power Electron. 2017, 6, 1553–1566.

[19]. Singh P, Purwar P. Sliding mode controller for PWM based Buck-Boost DC/DC converter as state space averaging method in continuous conduction mode. 2nd International Conference on Power, *Control and Embedded Systems (ICPCES)*; 2012.

[20]. H. Sadeghi and H. R. Mohammadi, “An improved fuzzy controlled back-to-back electric spring using hybrid structure of ES-1 and shunt-APF to improve power quality in micro- grids,” *International Journal of Industrial Electronics Control and Optimization*, vol. 5, no. 1, pp. 89–98, 2022.

[21]. S. R. Das, P. K. Ray, and A. Mohanty, “Fuzzy sliding mode based series hybrid active power filter for power quality enhancement,” *Advances in Fuzzy Systems*, vol. 2018, Article ID 1309518, 8 pages, 2018.

[22]. A. K. Mishra, P. K. Ray, R. K. Mallick, A. Mohanty, and S. R. Das, “Adaptive fuzzy controlled hybrid shunt active power filter for power quality enhancement,” *Neural Com- puting & Applications*, vol. 33, no. 5, pp. 1435–1452, 2021.

[23]. S. Echalih, A. Abouloifa, I. Lachkar et al., “A cascaded con- troller for a grid-tied photovoltaic system with three-phase half-bridge interleaved buck shunt active power filter: hybrid control strategy and fuzzy logic approach,” *IEEE Journal on Emerging and Selected Topics in Circuits and Systems*, vol. 12, no. 1, pp. 320–330, 2022.

[24]. X. Sun, D. Xu, F.H.F.Leung, Y.Wang, Y.S.Lee, “Design and implementation of a neural network controlled UPS inverter”, *IEEE/IECON*, Vol.2, pp.779-784, Nov. 1999.

[25]. D. Daniolos, M.K.Darwish, P.Mehta, “Optimized PWM inverter control using artificial neural networks”, *IEEE/PESC*, Vol.33, No.20, pp.1739-1740, Sep. 1995.

[26]. L.G.Barnes, R.Krishnan, "An adaptive three phase UPS inverter controller", *IEEE/PESC*, Vol.1, pp.473-479, June 1995.

[27]. Hasan Komurcugil; Sertac Bayhan; Ramon Guzman; Mariusz Malinowski. Design of Lyapunov Function Based Control For Power Converter, Page: 59 – 72, Edition: 1, *Wiley-IEEE Press*, 2023.DOI: 10.1002/9781119854432.ch4

[28]. Hasan Komurcugil; Sertac Bayhan; Ramon Guzman; Mariusz Malinowski. Design of Lyapunov Function-Based Control of Various Power Converters, Page: 261 – 308, Edition: 1, *Wiley-IEEE Press*, 2023.

[29]. Wenjie Ma, Bo Zhang, Dongyuan Qiu, Huadong Sun. Switching Control Strategy for DC–DC Converters Based on Polynomial Lyapunov Function and Sum-of-Squares Approach. 2022-06-07. *IEEE Transactions on Industrial Electronics* .DOI:10.1109/tie.2022.3179548.

[30]. H. Komurcugil, N. Guler, and S. Bayhan. Lyapunov-Function Based Control Strategy for Four-Switch Buck-Boost DC-DC Converters**.** 2022-06**.** *IEEE International Symposium on Industrial Electronics*. DOI: 10.1109/ISIE51582.2022.9831585.

[31]. S. Prakash, J. K. Singh, and R. K. Behera. Lyapunov function based control strategy for single-phase grid-connected PV system with LCL-filter**.** 2020-12**.** *9th IEEE International Conference on Power Electronics, Drives and Energy Systems*. DOI: 10.1109/PEDES49360.2020.9379547.

HARMONIC REDUCTION FOR SINGLE-PHASE UNINTERRUPTIBLE POWER SUPPLY INVERT

GIẢM SÓNG HÀI CHO BỘ BIẾN TẦN NGUỒN ĐIỆN MỘT PHA KHÔNG NGẮT

PHẠM TRẦN BÍCH THUẬN[1], NGUYỄN VINH QUAN[2], TRẦN THANH HẢI[3]*

[1] *Phòng Quản lý Khoa học và Hợp tác quốc tế, Đại học Công nghiệp Thành phố Hồ Chí Minh*

[2] *Khoa Công nghệ Điện tử, Đại học Công nghiệp Thành phố Hồ Chí Minh*

[3] *Phòng Kế hoạch Đầu tư, Đại học Công nghiệp Thành phố Hồ Chí Minh*

* *Tác giả liên hệ: quan_01037027@iuh.edu.vn*

Tóm tắt. Nhiều giải pháp điều khiển được áp dụng cho bộ biến tần của UPS đã được đề nghị với mục tiêu cơ bản của hệ thống điều khiển UPS (Uninterruptible Power Supply) là khả năng bám theo điện áp đặt, mức độ bền vững và duy trì dạng sóng điện áp hình sin hoàn hảo ngay cả với tải phi tuyến, tải thay đổi và có các thành phần bất định như nhiễu.

Một nguyên lý được đề nghị là hai vòng điều khiển MLC - Multiple feedback Loop Control bao gồm vòng ngoài điều khiển điện áp đo bám theo điện áp đặt và vòng trong điều khiển dòng điện để giảm sai số xác lập cho điện áp trên tải, giảm hài cho dòng điện trong mạch chính và làm tăng hiệu suất của hệ thống, độ bền vững của bộ điều khiển dựa vào hàm Lyapunov được chứng minh bởi sự thay đổi đột ngột của tải cũng như sự thay đổi của nguồn điện áp đặt cùng với sự hiện diện của nhiễu, các nguyên tắc cơ bản của định lý lyapunov được áp dụng vào các phương trình trạng thái dẫn đến việc tính toán hàm chuyển mạch để tạo xung PWM (Pluse Width Modulation) để giảm hài cho UPS.

Mô phỏng và thực nghiệm được phát triển trên Matlab-Simulink. Kết quả cho thấy điện áp và dòng điện đầu ra của UPS sẽ bám theo giá trị đặt từ thấp đến cao bất chấp sự thay đổi đột ngột của tải cũng như điện áp đặt cùng với sự hiện diện của nhiễu, giảm đáng kể sóng hài THD (THD- Total Harmonic Distortion) hiện tại xuống còn 0.04%, thỏa tiêu chuẩn IEEE-519.

Từ khóa. Bộ nguồn liên tục, Biến tần ba cấp, Lyapunov.

Received on Feb 24– 2025

Revised on March 24 – 2025